IEEE Robotics and Automation Letters (RAL) paper presented at
2024 IEEE/RSJ International Conference on Intelligent Robots and Systems (IROS)
October 14-18, 2024. Abu Dhabi, UAE

Optimizing Setup Configuration of a Collaborative Robot Arm-based Bimanual Haptic Display for Enhanced Performance

Joong-Ku Lee, and Jee-Hwan Ryu

***Abstract*— A bimanual haptic display supporting the full range of human arm motion and providing a sufficient haptic feedback force/torque is essential for achieving human-like manipulation in remote or virtual environments. This paper proposes the use of redundant collaborative robot arms as a bimanual haptic display and introduces an optimization scheme to determine its optimal setup configuration. The scheme considers factors including human arm workspace coverage, redundancy, renderable haptic feedback force/torque, and potential collisions with a human arm. The proposed optimization scheme is applied to the Panda and iiwa 7 robot arms and the results are compared to the setup configurations of NimbRo and German Aerospace Center (DLR) HUG. The optimized setup configurations with the proposed scheme were observed to outperform the existing setup configurations.**

I. Introduction

The recent COVID-19 pandemic and the emergence of metaverse trends have sparked renewed interest in teleoperation and haptic-enabled interactions with extended reality (XR) environments. These technologies enable individuals to explore and interact with remote or virtual environments, even if they are not physically present. While prominent advances in autonomous robot control have been reported, human manipulation and interactive control skills, including the execution of COVID-19 rapid antigen tests, or the interaction with various objects in XR environments, cannot be replicated easily.

To achieve human-like manipulation services during pandemics and enable full-immersive interaction with XR environments, a bimanual haptic display is indispensable. Moreover, it must cover the entire range of human arm motion to support the seamless execution of any intended human motions. Techniques such as indexing [1] and scaling [2] that are used to overcome workspace limitations are not ideal for bimanual manipulation because they considerably reduce transparency.

Currently, it is hard to find an off-the-shelf bimanual haptic display that covers the entire human arm workspace and provides sufficient feedback force/torque. While it's possible to configure a bimanual haptic display using two commercially available devices, these are typically desktop systems with limited workspace and feedback force/torque range, presenting challenges for bimanual manipulation tasks. Existing devices that cover the entire human arm workspace often demand a nearly room-sized space and are less practical. Some researchers have developed exoskeletons for bimanual haptic display [3], [4]; however, these are not commercially available. Additionally, prototyping a bimanual haptic display is a time-consuming and resource-intensive process. This not only hinders researchers from replicating, repairing, and operating but also impedes rapid technological advancement in this field.

Meanwhile, there have been efforts to utilize commercially available redundant collaborative robot arms as a bimanual haptic display, given their similar joint configuration, workspace, and force/torque capabilities to those of the human arm. Researchers at the German Aerospace Center (DLR) have built a bimanual haptic display using two DLR/KUKA LWR arms [5], [6], and the winning team of the ANA Avatar XPRIZE, NimbRo, has developed a bimanual haptic display using Franka Emika Panda robot arms [7].

As established in prior works [8], [9], [10], the determination of an optimal robot base pose to enhance robot performance has been a long-standing challenge in the field of robotics. In the specific context of bimanual haptic displays with two robot arms, precise determination of the robot arm base poses is crucial, as it significantly impacts haptic display performance, including workspace and feedback force/torque. A prior study investigated two different setup configurations of a robot arm-based bimanual haptic display [6]. However, this study was limited to a simple comparison between two different setup configurations based on human palm pose reachability. More Recently, an optimization-based approach was proposed to find the optimal setup configuration for robot arms in a bimanual haptic display [7], [11]. Nevertheless, the approach was limited to maximizing reachability and did not account for critical factors such as human- and robot-arm collisions or renderable haptic feedback force/torque.

This paper presents an optimization scheme for determining the optimal setup configuration of a robot arm-based bimanual haptic display. Our approach distinguishes itself from prior research by comprehensively considering crucial factors for the haptic display, including reachability, redundancy, renderable haptic feedback force/torque of robot arms, and potential human and robot arm collisions. We apply this optimization scheme to two widely used collaborative robots, Franka Emika Panda and KUKA iiwa 7, and compare the performance of the bimanual haptic display using our optimized setup configuration against previously proposed

This research was supported in part by the Field-oriented Technology Development Project for Customs Administration through National Research Foundation of Korea(NRF) funded by the Ministry of Science & ICT and Korea Customs Service(2022M3I1A109507521) and in part by the Robot Industry Core Technology Development Program (20023294) funded By the Ministry of Trade, Industry & Energy(MOTIE, Korea)

Authors are with the Department of Civil and Environmental Engineering, Korea Advanced Institute of Science and Technology, Daejeon 34141, South Korea. {iamjoong9, jhryu}@kaist.ac.kr

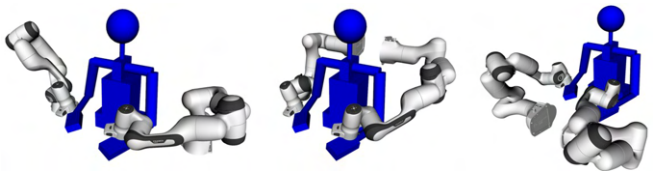

Fig. 1: Robot arm-based haptic display with various robot arm base poses. Several robot arm base poses are possible and configurations of the robot arms are drastically altered by simply changing the robot arm base poses.

setup configurations.

The paper is structured as follows. Section II outlines the design variables and requirements for bimanual haptic displays. Section III presents the kinematic model of a human arm and its workspace analysis. The design factors, objective function, and implementation details of the optimization are explained in Section IV. Section V presents the optimization results obtained using two different commercialized robot arms and their comparison with other existing setup configurations. Finally, Section VI concludes this paper.

II. Problem Statement

A. Design Variables

As shown in Fig. 1, a slight variation of the robot base poses cause large configuration changes of the robot arm-based bimanual haptic display. Assuming diverse setup configurations impact the performance of the bimanual haptic display, we defined the design variables associated with the position and orientation of the robot arm bases as $X_b \in \mathbb{R}^3$ and $R_b \in \mathbb{R}^3$, respectively. X_b is a translational offset from the human pelvis to the robot base, and R_b represents the roll-pitch-yaw orientation of the robot arm base relative to the human pelvis. To simplify the analysis, the robot arm base poses were assumed to have reflection symmetry about the sagittal plane of humans. Therefore, only the left robot arm base's position and orientation are considered for optimization, with the right arm base automatically determined. This mirror-symmetric base setup may not result in symmetric configurations of the robot arms and lead to asymmetry in robot dynamics. However, we disregarded these effects as they have a negligible impact on the operator.

Additionally, as shown in Fig. 2, several grab angles between the robot end-effector and human palm are possible and we assumed that this grab angle could affect the performance. Accordingly, we include the grab angle θ_{grab} as an additional design variable for optimization. Assuming reflection symmetry in grab angles for left and right palms, we define only the grab angle for the left human palm.

B. Requirements of Bimanual Haptic Displays

The proposed optimization scheme aimed to identify the optimal set of design variables, namely X_b, R_b, and θ_{grab}, to achieve maximum bimanual haptic display performance. To ensure optimal performance, certain (general) requirements for bimanual haptic displays must be met.

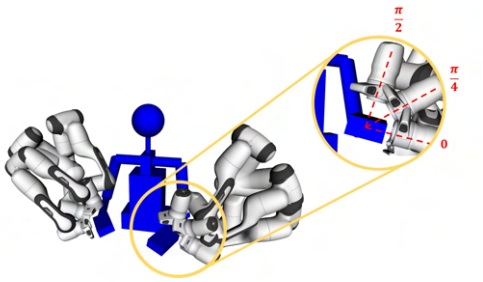

Fig. 2: Alteration of the grab angle between the human palm and robot arm end-effector causes large configuration changes even when the bases of the robot arm are fixed.

Firstly, the bimanual haptic display should cover the entire workspace of the human arm, allowing unrestricted manipulation movements without disturbing the operator. Full coverage of available human poses is necessary, as no specific task is targeted in this study. Additionally, robot arm redundancy in human-available poses is essential to facilitate dexterous arm and hand movements while avoiding collisions between the human and robot arms.

Secondly, the bimanual haptic display must provide sufficient haptic feedback forces/torques in all directions and under any circumstances. As the study does not focus on a specific task, the optimized robot arm-based bimanual haptic display should withstand the maximum isotropic worst-case haptic feedback force/torque that the human operator could apply in any available pose.

III. Human Arm Kinematics

A. Kinematic Model

Fig. 3a and 3b show the kinematic model of a human arm including the upper body, left arm, and right arm. The human arm was modeled as a seven-joint serial manipulator [12], with the left and right arms sharing the same Denavit–Hartenberg (DH) parameters but having different joint limits. Anthropometric dimensions of the arm are defined based on the individual with median height from a group of eight individuals in [13] to ensure the generality of the human kinematic model and the setup configuration's robustness to anthropometric variations. Consequently, the link lengths of the shoulder, upper arm, lower arm, and palm were set to $l_{sh} = 0.163\,m$, $l_{ua} = 0.315\,m$, $l_{la} = 0.258\,m$, and $l_p = 0.05\,m$, respectively. The diameters of the upper arm and lower arm were set to $0.068\,m$ and $0.046\,m$, respectively. The neck and torso joints were considered fixed in this study, assuming that the connections between robot arm base frames remained fixed relative to the human pelvis frame during bimanual operation.

B. Workspace

Analysis of the human arm workspace was performed using the provided human kinematic model. To assess the human arm workspace, we examined the existence of inverse kinematics (IK) solutions for a given discretized pose around the human operator. The discretized positions were obtained via equidistant sampling of the workspace around the human

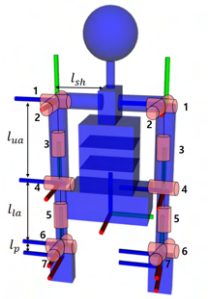

(a)

Joint i	DH Parameters a	α	d	θ	Joint Limits Left min	Left max	Right min	Right max
1	0	90°	0	90°	−30°	180°	−30°	180°
2	0	90°	0	90°	−90°	50°	−50°	90°
3	0	−90°	$-l_{ua}$	0	−80°	80°	−80°	80°
4	0	90°	0	0	0°	160°	0°	160°
5	0	90°	$-l_{la}$	−90°	−85°	90°	−90°	85°
6	0	−90°	0	90°	−85°	85°	−85°	85°
7	$-l_p$	0	0	0	−15°	45°	−45°	15°

(b)

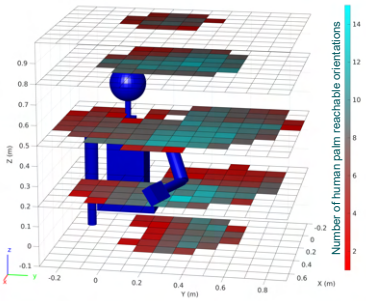

(c)

Fig. 3: (a) Illustration of the human arm kinematic model. (b) DH parameters of the human arm model, which are shared by the left and right arms with different joint limits. (c) Visualization of the left human arm workspace $\mathbb{T}_L^h$. The colormap on each position is determined by the number of human palm reachable orientations among 50 discretized orientations.

operator, while the uniformly discretized orientations were generated based on the super-Fibonacci algorithm [14]. In this study, the position was discretized with a fixed step size $0.1\,m$, and 50 orientations were sampled at each position. It should be noted that the choice of the step size and the number of orientations is the main factor influencing the total computation time and involves a trade-off between computation time and optimization result. The resulting set of discretized query poses around the human operator was defined as $\mathbb{T}_S = \mathbb{T}_P \times \mathbb{T}_R \subset SE(3)$, where $\mathbb{T}_P$ and $\mathbb{T}_R$ are the set of discretized positions and orientations, respectively.

After the definition of the set of query poses $\mathbb{T}_S$, the human arm workspace was analyzed by computing the IK solutions for each human arm at each query pose $T_S \in \mathbb{T}_S$. As the human arm is a kinematically redundant system with seven joints, multiple IK solutions were derived at various elbow positions. Subsequently, physically feasible solutions (which did not result in collisions with the human body) were identified among the calculated IK solutions. Finally, the most suitable human arm configuration for a given pose was determined by selecting the solution with the highest manipulability index [15]. We did not consider the continuity in the human joint space as this analysis merely required possible joint configurations of the human arm to reach discrete poses and was not used to achieve continuous movements of the human arm.

For each query pose T_S, either an empty or a single IK solution for the left and right human arms were obtained and respectively denoted as $Q_L^h(T_S)$ and $Q_R^h(T_S)$. Subsequently, the sets of reachable poses for the left and right human palms, represented as $\mathbb{T}_L^h$ and $\mathbb{T}_R^h$, respectively, were determined by including the query pose T_S for which an IK solution existed. Thus, the sets $\mathbb{T}_L^h$ and $\mathbb{T}_R^h$ became subsets of the $\mathbb{T}_S$, specifically comprising the poses that can be reached by the left and right human palms. For each pose $T_L^h \in \mathbb{T}_L^h$ and $T_R^h \in \mathbb{T}_R^h$, the corresponding configurations of the left and right human arm joints were defined as $Q_L^h(T_L^h)$ and $Q_R^h(T_R^h)$ respectively.

IV. Optimization

A. Design Factors

The optimal setup configuration of the robot arms for a bimanual haptic display must satisfy the requirements outlined in Section II-B, including full and redundant coverage of the human arm workspace, collision-free operation, and satisfactory feedback forces/torques to the human operator. This subsection discusses the design factors to be considered and explains how they are calculated for each setup configuration. For simplicity, the procedure is explained with the left human and robot arms.

1) Workspace Coverage: To analyze the bimanual haptic display with the specified setup configuration, we first calculated the IK solutions of the robot arm for the reachable poses of the human palm $\mathbb{T}_L^h$. As the robot arm used in this study was assumed to be kinematically redundant, multiple IK solutions were available for each pose. To obtain all the possible solutions, we discretized the joint angle of a free joint equally between its joint limits. In this study, the free joint was equally discretized to 100 different angles. Consequently, the empty or multiple IK solutions of the robot arm for all reachable poses of the human palm $\mathbb{T}_L^h$ were obtained. As a result, the IK solutions of the robot arm for each reachable pose of the human palm $T_L^h \in \mathbb{T}_L^h$ were defined as $\mathbb{Q}_L^r(T_L^h)$ (Fig. 4a).

To ensure real-world safety and feasibility, it is essential to obtain robot arm IK solutions that do not result in any collision with the human arm or body. Thus, we utilized the joint configuration of the human arm which was defined as $Q_L^h(T_L^h)$ in Section III-B. Among all the possible joint configurations of the robot arm $\mathbb{Q}_L^r(T_L^h)$, we identified the IK solutions that did not induce any collision with the human body or arm. Finally, we obtained the IK solutions of the robot arm for the reachable pose of the human palm T_L^h that did not cause any collision with the human operator. These collision-free IK solutions were defined as $\mathbb{Q}_L^{r,cf}(T_L^h)$ (see Fig. 4b).

2) Renderable Haptic Feedback Force/Torque: Each commercialized robot arm has its own torque limit for each joint. Within the joint torque limit of a given robot arm, the robot arm-based bimanual haptic display with an optimized

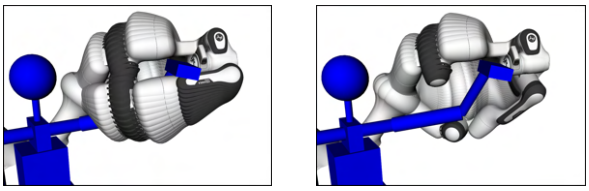

(a) (b)

Fig. 4: Procedure for workspace coverage analysis. (a) All IK solutions of the robot arm are calculated to reach the considered human palm pose. (b) Among the resulting robot joint configurations given in (a), the configurations that do not induce collision with the human arm and body are identified.

setup configuration should be able to render the largest possible feedback force/torque while 1) continuously exerting gravitational torque to maintain its posture and 2) providing human operator arm weight compensation torque so that the human operator can interact with the display comfortably. The human arm weight compensation torque is included in this study because operators easily get fatigued without the support of their arm weight, especially during long-term operations. Considering this aspect, this subsection discusses the procedure used to determine the maximum applicable haptic feedback force/torque of the robot arm in the given setup configuration and robot arm joint configurations.

Given the collision-free joint configurations of the robot arm $\mathbb{Q}_L^{r,cf}(T_L^h)$ for each possible human palm pose T_L^h, the haptic feedback force/torque coverage of the robot arm on T_L^h was analyzed by calculating the maximum applicable haptic feedback force/torque of all possible joint configurations $Q_L^{r,cf}(T_L^h) \in \mathbb{Q}_L^{r,cf}(T_L^h)$.

First, the gravity compensation torque of the robot arm was calculated using the robot dynamics model, and the resulting torque was defined as $\tau_{grav}(Q_L^{r,cf}(T_L^h))$. Second, the joint torque of the robot arm required to compensate for the human arm weight was defined as $\tau_{arm}(Q_L^{r,cf}(T_L^h))$, which was calculated as

$$\tau_{arm}(Q_L^{r,cf}(T_L^h)) = -J(Q_L^{r,cf}(T_L^h))^T \cdot F_{arm}, \quad (1)$$

where $J(Q_L^{r,cf}(T_L^h))$ is a Jacobian matrix calculated using the kinematic chain of the robot arm from its base to the human palm frame in the robot joint configuration $Q_L^{r,cf}(T_L^h)$. F_{arm} is the force/torque vector of the human arm weight represented in the human pelvis frame; in this study, the magnitude of this vector was set to $-20\,N$, and its direction was along the z-axis.

Third, the analysis of the maximum renderable haptic feedback force/torque proceeded toward the calculation of the remaining robot joint torque margin τ_{ft} after the application of the gravity and human-arm-weight compensation torques to the robot arm as

$$\tau_{ft} = \tau_{limit} - \|\tau_{grav} + \tau_{arm}\|, \quad (2)$$

where τ_{limit} denotes the positive joint torque limit of the considered robot arm. Finally, the maximum applicable haptic feedback force/torque that can cover all directions on the human palm frame with robot joint configuration $Q_L^{r,cf}(T_L^h)$ was calculated as

$$\begin{aligned} F_{max}(Q_L^{r,cf}(T_L^h)) &= \min(\tau_{ft} \oslash \|J_v(Q_L^{r,cf}(T_L^h))^T \cdot d_v\|), \\ T_{max}(Q_L^{r,cf}(T_L^h)) &= \min(\tau_{ft} \oslash \|J_\omega(Q_L^{r,cf}(T_L^h))^T \cdot d_\omega\|), \end{aligned} \quad (3)$$

where $\min$ operator extracts the minimum value of the given vector, $\oslash$ is a notation for the element-wise division of vectors, and $J_v(Q_L^{r,cf}(T_L^h))$ and $J_\omega(Q_L^{r,cf}(T_L^h))$ comprise the top and bottom three rows of $J(Q_L^{r,cf}(T_L^h))$, respectively. d_v and d_ω are the force and torque directions, respectively, that result in the maximum magnitude of the robot joint torques. They were calculated by performing singular value decomposition of $J_v(Q_L^{r,cf}(T_L^h))$ and $J_\omega(Q_L^{r,cf}(T_L^h))$ as

$$\begin{aligned} J_v(Q_L^{r,cf}(T_L^h)) &= U_v S_v V_v^T, \\ J_\omega(Q_L^{r,cf}(T_L^h)) &= U_\omega S_\omega V_\omega^T, \end{aligned} \quad (4)$$

and extracting the first-column vectors of U_v and U_ω, respectively.

Using the aforementioned procedure, we calculate the maximum renderable haptic feedback forces and torques for all possible robot joint configurations to reach the desired human palm pose T_L^h. Subsequently, the renderable haptic feedback force/torque of a specified human palm pose was established as the minimum value among the calculated maximum applicable haptic feedback forces and torques and defined as $F_{max}(T_L^h)$ and $T_{max}(T_L^h)$.

B. Objective Function

Finally, the robot arm's collision-free configurations and the renderable haptic feedback force/torque for each human palm reachable pose are calculated in the given setup configuration. To evaluate the given setup configuration, the objective function was designed to consider equally the workspace coverage and haptics performance. The objective function was set as

$$O = S_{workspace} + S_{haptics}, \quad (5)$$

and the optimization goal was set to maximize the formulated objective function.

$S_{workspace}$ was designed to optimize the bimanual haptic display to maximize the robot arm capability to cover as many human-reachable poses as possible while providing a broad range of redundancy to easily accommodate dexterous human movements. The equation for $S_{workspace}$ can be expressed as,

$$\begin{aligned} S_{workspace} = &\sum_{T_L^h \in \mathbb{T}_L^h} \sigma(|\mathbb{Q}_L^{r,cf}(T_L^h)|) + \sigma(\frac{|\mathbb{Q}_L^{r,cf}(T_L^h)|}{\mathfrak{I}}) \\ &+ \sum_{T_R^h \in \mathbb{T}_R^h} \sigma(|\mathbb{Q}_R^{r,cf}(T_R^h)|) + \sigma(\frac{|\mathbb{Q}_R^{r,cf}(T_R^h)|}{\mathfrak{I}}), \end{aligned} \quad (6)$$

where σ is a saturation function defined as

$$\sigma(x) = \begin{cases} 0 & \text{if } x < 0 \\ x & \text{if } 0 \le x < 1 \\ 1 & \text{else.} \end{cases} \quad (7)$$

$|\mathbb{Q}|$ returns the number of elements in $\mathbb{Q}$, and $\mathfrak{I}$ is the maximum number of IK results, which were defined when the joint angle of the free joint was discretized, as explained in Section IV-A.1. Using this objective function, a score of one was assigned when the robot successfully achieved a given human-reachable pose, and additional scores were assigned based on the proportion of redundant solutions.

$S_{haptics}$ was defined to ensure that the optimized bimanual haptic display could provide sufficient haptic feedback force/torque to the human operator. $S_{haptics}$ can be expressed as

$$S_{haptics} = \sum_{T_L^h \in \mathbb{T}_L^h, Q_L^h \in \mathbb{Q}_L^h} \sigma(\frac{F_{max}(T_L^h)}{\mathfrak{F}}) + \sigma(\frac{T_{max}(T_L^h)}{\mathfrak{T}}) + \sum_{T_R^h \in \mathbb{T}_R^h, Q_R^h \in \mathbb{Q}_R^h} \sigma(\frac{F_{max}(T_R^h)}{\mathfrak{F}}) + \sigma(\frac{T_{max}(T_R^h)}{\mathfrak{T}}), \tag{8}$$

where $\mathfrak{F}$ and $\mathfrak{T}$ are constants representing the maximum applicable human force and torque, respectively. Any renderable haptic feedback force/torque exceeding these parameters will be saturated, contributing maximally to $S_{haptics}$. Therefore, low $\mathfrak{F}$ and $\mathfrak{T}$ will lead to $S_{haptics}$ being easily saturated, thus resulting in an optimized setup configuration focused on workspace coverage and redundancy. In this study, $\mathfrak{F}$ and $\mathfrak{T}$ were set to $100\,N$ and $10\,Nm$, respectively. We experimentally identified these values by measuring the maximal human resistible force/torque using a sensor. This was done during operator interaction with a robot arm in a neutral configuration, gradually increasing the applied force and torque until the operator could not maintain their initial position. However, these parameters can be customized for the human operator, and such optimization will lead to a more optimal setup configuration tailored to the operator.

C. Implementation

Finding the global maximum of (5) is challenging due to the non-linear, non-convex nature of our problem. To find the optimum point amid the numerous local optima resulting from various setup configurations, we employed a global optimization algorithm. Among several options, we chose a particle swarm algorithm for its computational efficiency. It's crucial to note that using a global optimization algorithm doesn't guarantee convergence to the global optimum. However, we made efforts to maximize the likelihood of reaching this point. This involved configuring a larger swarm size, a smaller neighborhood size, and conducting multiple optimization runs to fully leverage the inherent randomness of the particle swarm algorithm.

The main optimization process was implemented in MATLAB using the Global Optimization Toolbox. The SwarmSize parameter was set to 100 and the MinNeighborsFraction parameter was set to 0.1. To reduce the search space, the lower and upper bounds of the design variables were set to $(-1.0,\ 0.0,\ -0.5) \leq X_b \leq (1.0,\ 0.8,\ 1.0)$, $(-\frac{\pi}{2},\ 0,\ -\pi) \leq R_b \leq (0,\ \frac{\pi}{2},\ \pi)$, $-\frac{\pi}{2} \leq \theta_{grab} \leq \frac{\pi}{2}$. The procedure to calculate the objective function for the given setup configuration was conducted in C++ to improve time efficiency. IKFast (OpenRAVE [16]) was used to obtain fast and reliable analytic IK solutions for the robot and human arms. The collision between the robot and human was verified using MoveIt [17], whereas the KDL library [18] was used to calculate the gravitational torque τ_{grav} of the robot arm.

V. Optimization Results

The optimization was performed on an Intel NUC equipped with an Intel i5-1135G7 CPU (4 cores). The runtime of each optimization was in the range of 5-44 h (a total of 40 optimizations), and the average runtime was 21.18h. The optimization result with the highest objective function value was selected and examined in this study.

A. Application to Franka Emika Panda Robot Arm

The proposed setup configuration optimization scheme was applied to the Franka Emika Panda robot arm [19].

TABLE I: Optimized design variables with the Panda robot arms.

Design Variables	Values	Units
Base Position (X_b)	(-0.205, 0.066, 0.262)	m
Base Orientation (R_b)	(-0.900, 0.177, -0.219)	rad
Grab Angle (θ_{grab})	-0.569	rad

Table I lists the design variables, including the base position, base orientation, and grab angle for the robot arm on the left side, derived from the optimization process. The objective function O achieved a maximum optimized value of 11681.95 with the values of $S_{workspace}$ and $S_{haptics}$ of 5441.11 and 6240.84, respectively. The optimized setup configuration of the Panda robot arm-based bimanual haptic display is illustrated in Fig. 5a. The optimized configuration located the robot arm bases on the back of the human operator in a tilted manner. The grab angle was derived such that the end-effector of the robot arm was positioned on the side beneath the human palm.

To validate the proposed setup configuration, we compared its performance with that of NimbRo's bimanual haptic display, the winner of the ANA Avatar XPRIZE. The setup configuration of NimbRo's bimanual haptic display with the Panda robot arm was replicated, as shown in Fig. 6a, with its parameters defined as $X_b = (-0.282,\ 0.4,\ 0.69)\,m$, $R_b = (-2.28,\ 0,\ -1.23)\,rad$, and $\theta_{grab} = 1.57\,rad$. We evaluated the workspace coverage, average redundancy, and renderable haptic feedback force/torque of both setup configurations.

As shown in Fig. 5b and 6b, the proposed setup configuration provided coverage for a majority of the workspace, with a small exception of positions on the opposite side and near the second joint of the robot arm. Conversely, NimbRo's setup configuration had a smaller workspace coverage, particularly for the human arm workspace underneath the pelvis, overhead, and around the shoulder. Additionally, the results in Figs. 5c and 6c indicate that the proposed setup configuration had greater kinematic redundancy in the human palm

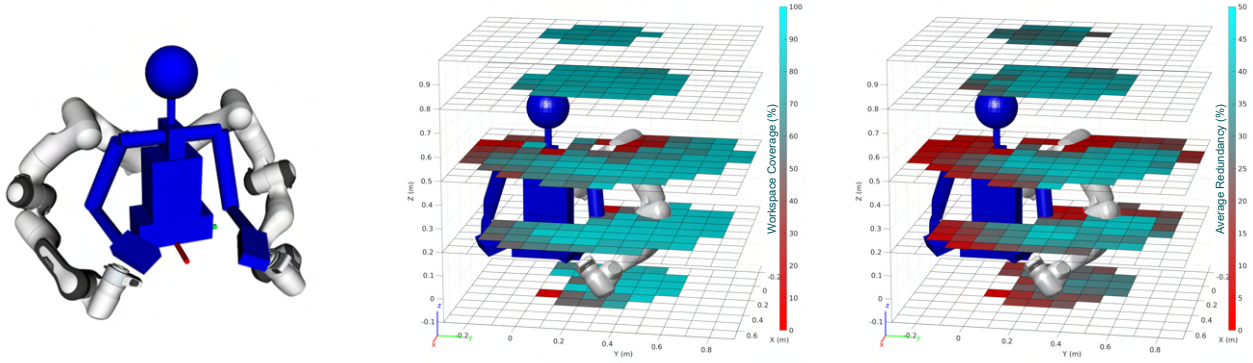

(a) Proposed setup configuration (b) Workspace coverage (c) Average redundancy

Fig. 5: (a) Visualization of the Panda robot arm-based bimanual haptic display with the proposed optimized setup configuration. (b) Workspace coverage of the left robot arm to cover the left human palm reachable poses. (c) Average redundancy of the left robot arm to cover the left human palm reachable poses.

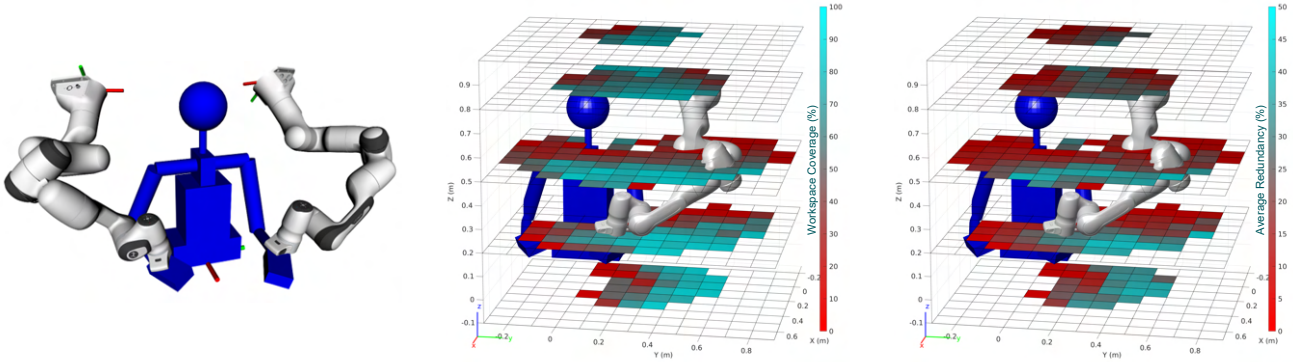

(a) Team NimbRo's setup configuration (b) Workspace coverage (c) Average redundancy

Fig. 6: (a) Visualization of the Panda robot arm-based bimanual haptic display with team NimbRo's setup configuration. (b) Workspace coverage of the left robot arm to cover the left human palm reachable poses. (c) Average redundancy of the left robot arm to cover the left human palm reachable poses.

workspace. Thus, the human operator using the bimanual haptic display with the proposed setup configuration could perform common manipulation tasks with greater dexterity.

TABLE II: Panda robot arm - Performance comparison between the proposed and Nimbro's setup configurations.

Performance Index	**NimbRo's**	**Proposed**
Workspace Coverage	63.77 %	86.13 %
Average Redundancy	22.09 %	35.11 %
Average Force Feedback	68.69 N	74.72 N
Average Torque Feedback	10.40 Nm	9.94 Nm

A quantitative comparison of the two setup configurations is presented in Table II. The results demonstrated that the proposed setup configuration outperformed NimbRo's setup configuration in terms of meeting the general requirements for bimanual haptic displays, including workspace coverage, average redundancy, and renderable haptic feedback force. While renderable haptic feedback torque slightly decreased, it remained around the maximum human-renderable torque value, $\mathfrak{T} = 10\,Nm$.

In addition, it is worth noting that despite the asymmetry in the joint angle limits of the fourth and sixth joints of the Panda robot arm, our assessment indicated a minimal impact on performance. Specifically, our analysis revealed that the workspace coverage and average redundancy difference between the left and right robot arms were only 1.28% and 0.01%, respectively. These findings substantiate that the asymmetry in the joint limits in the mirror-symmetric setup configuration of the Panda robot arm has limited influence on its overall performance.

B. Application to KUKA LBR iiwa 7 Robot Arm

The proposed optimization scheme was applied to the KUKA LBR iiwa 7 robot arm [20]. The iiwa 7 robot arm exhibits greater joint angle limits and higher torque limits compared to the Panda robot arm. However, unlike the Panda robot arm, whose elbow joint (fourth joint) could almost fold fully, the iiwa 7 robot arm could only fold its elbow joint up to 120° in both directions. This kinematic limitation of the iiwa 7 robot arm made the robot end-effector unable to reach the $800mm$ diameter sphere-shaped workspace around the second joint of the iiwa 7 robot arm. Therefore, the workspace coverage of the bimanual haptic display with the iiwa 7 robot arm was expected to be inferior to that of the

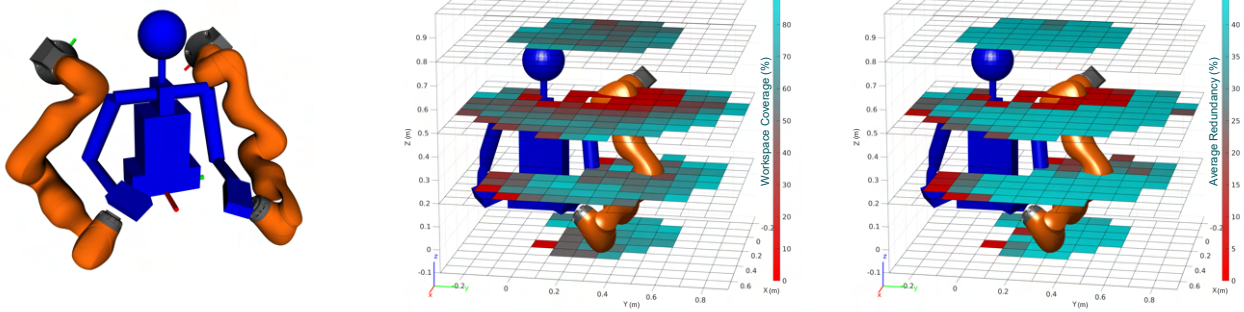

(a) Proposed setup configuration (b) Workspace coverage (c) Average redundancy

Fig. 7: (a) Visualization of the iiwa 7 robot arm-based bimanual haptic display with the proposed optimized setup configuration. (b) Workspace coverage of the left robot arm to cover the left human palm reachable poses. (c) Average redundancy of the left robot arm to cover the left human palm reachable poses.

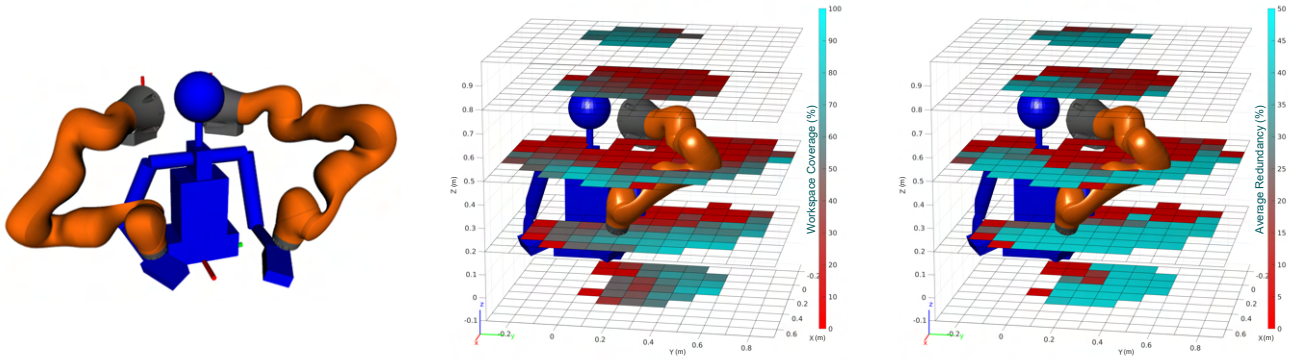

(a) DLR HUG's setup configuration (b) Workspace Coverage (c) Average redundancy

Fig. 8: (a) Visualization of the iiwa 7 robot arm-based bimanual haptic display with DLR HUG's setup configuration. (b) Workspace coverage of the left robot arm to cover the left human palm reachable poses. (c) Average redundancy of the left robot arm to cover the left human palm reachable poses.

bimanual haptic display using the Panda robot arm.

TABLE III: Optimized design variables with the iiwa 7 robot arm.

Design Variables	Values	Units
Base Position (X_b)	(-0.435, 0.369, 0.462)	m
Base Orientation (R_b)	(-1.537, 0.780, -1.782)	rad
Grab Angle (θ_{grab})	-0.408	rad

The design variables for the iiwa 7 robot arm-based bimanual haptic display obtained through optimization are presented in Table III. The objective function O was maximized at 10935.24 with $S_{workspace} = 5184.24$ and $S_{haptics} = 5751$, and the optimized setup configuration for the iiwa 7 robot arm-based bimanual haptic display is shown in Fig. 7a. Due to the kinematic limitations, the objective function O was lower than that obtained for the Panda robot arm. The optimization results also indicated that the haptic performance score $S_{haptics}$ for the iiwa 7 robot arm was lower than that for the Panda robot arm, despite the significantly higher joint torque limit of the iiwa 7 robot arm. This is because $S_{haptics}$ only increases when the robot can reach human palm-accessible poses, which was less likely with the iiwa 7 robot arm owing to its kinematic limitations.

The validation of the proposed setup configuration with the iiwa 7 robot arm was conducted by comparing the performance indices with the setup configuration of the DLR HUG bimanual haptic display. The setup configuration of the HUG was replicated, as shown in Fig. 8a, with parameters $X_b = (-0.3, 0.15, 0.55)\,m$, $R_b = (-1.57, -1.57, -0.785)\,rad$, and $\theta_{grab} = 1.57\,rad$.

Visualizations of the workspace coverage for the proposed and HUG's setup configurations of the left robot arm are presented in Figs. 7b and 8b, respectively. The joint angle limit of the fourth joint resulted in an unreachable workspace near the second joint of the robot arm for both cases. However, the proposed setup configuration minimized the overlap between the unreachable workspace of the robot arm and the human palm-available workspace, while a significant overlap was observed in HUG's setup configuration. Additionally, Fig. 7c and 8c present the average redundancy for the proposed and HUG's setup configurations, respectively. Owing to its larger joint limit, the iiwa 7 robot arm-based bimanual haptic display generally exhibited greater redundancy compared with that of the Panda robot arm-based display. Additionally, the proposed setup configuration showed significantly larger

average redundancy throughout the workspace compared with that of the HUG's setup configuration.

TABLE IV: iiwa 7 robot arm - Performance comparison between the proposed and DLR HUG's setup configurations.

Performance Index	DLR HUG's	Proposed
Workspace Coverage	43.68 %	63.98 %
Average Redundancy	64.74 %	73.06 %
Average Force Feedback	195.99 N	210.17 N
Average Torque Feedback	38.84 Nm	39.30 Nm

Table IV presents a quantitative comparison of the two setup configurations. Compared with the Panda robot arm-based bimanual haptic display, the iiwa 7 robot arm-based bimanual haptic display exhibited lower performance in terms of workspace coverage but excelled in redundancy and haptic feedback force/torque. Compared with the HUG's setup configuration, our proposed setup configuration significantly improved the workspace coverage, redundancy, and feedback force/torque.

C. Discussion

Although the case studies conducted to validate the effectiveness of our approach are presented with popular robot arms, such as Franka Emika Panda and Kuka iiwa7, the optimization scheme proposed in our work is not limited to particular robot arms but can be applied to any type of off-the-shelf collaborative robot arm. This versatility is possible because our scheme only requires a robot arm kinematic model and gravity vector, which are available for most off-the-shelf collaborative robot arms.

Additionally, even though we conducted optimizations with the generalized human kinematic model, utilizing specific anthropometric measurements of the individual human operator will lead to the most optimal setup configuration tailored to the operator. Nevertheless, the optimized setup configuration for the individual used in this study shows insensitive performance to various human kinematic models as the performance index evaluated with the individuals with the biggest and smallest anthropometric measurements in [13] only decreased by 1.06 % and 0.58 % on average compared with their optimized setup configurations.

VI. Conclusion

This study presents an optimization scheme to determine the optimal setup configuration of a robot arm-based bimanual haptic display. The proposed optimization scheme determined the robot arm base poses and grab angle to maximize simultaneously the workspace coverage, redundancy, and renderable haptic feedback force/torque of the robot arm while considering the human arm workspace and collision. We demonstrated that the bimanual haptic display with the proposed optimized setup configuration (which utilized the Panda and iiwa 7 robot arms) outperformed the team NimbRo's and DLR HUG's setup configurations.

Nevertheless, it is important to note that our proposed optimization scheme primarily emphasized generalized bimanual operations rather than specific bimanual tasks. To overcome this limitation, the scheme could be further enhanced by incorporating actual bimanual task demonstrations. This can be achieved by acquiring query poses and continuous human arm joint configurations from the bimanual task demonstrations using a motion capture system and optimizing with this data. Additionally, assigning higher weights to workspace visited frequently during optimization and considering the collisions between robot arms during the optimization process would lead to a more optimal setup configuration for a specific task.

References

[1] E. G. Johnsen and W. R. Corliss, *Human factors applications in teleoperator design and operation*. Wiley-Interscience New York, 1971.

[2] J. Yan and S. E. Salcudean, "Teleoperation controller design using H_∞-optimization with application to motion-scaling," *IEEE Trans. CST*, vol. 4, no. 3, pp. 244–258, 1996.

[3] M. Mallwitz *et al.*, "The capio active upper body exoskeleton and its application for teleoperation," in *Proceedings of the 13th Symposium on Advanced Space Technologies in Robotics and Automation*, 2015.

[4] C. Carignan, J. Tang, and S. Roderick, "Development of an exoskeleton haptic interface for virtual task training," in *IEEE/RSJ IROS*, 2009, pp. 3697–3702.

[5] T. Hulin *et al.*, "The dlr bimanual haptic device with optimized workspace," in *IEEE ICRA*, 2011, pp. 3441–3442.

[6] F. Zacharias, I. S. Howard, T. Hulin, and G. Hirzinger, "Workspace comparisons of setup configurations for human-robot interaction," in *IEEE/RSJ IROS*, 2010, pp. 3117–3122.

[7] C. Lenz and S. Behnke, "Bimanual telemanipulation with force and haptic feedback and predictive limit avoidance," in *European Conference on Mobile Robots (ECMR)*. IEEE, 2021, pp. 1–7.

[8] D. Hsu *et al.*, "Placing a robot manipulator amid obstacles for optimized execution," in *IEEE international symposium on assembly and task planning*, 1999, pp. 280–285.

[9] Urakubo *et al.*, "Optimal placement of a two-link manipulator for door opening," in *IEEE/RSJ IROS*, 2009, pp. 1446–1451.

[10] L. Adhami and E. Coste-Maniere, "Positioning tele-operated surgical robots for collision-free optimal operation," in *IEEE ICRA*, 2002, pp. 2962–2967.

[11] C. Lenz and S. Behnke, "Bimanual telemanipulation with force and haptic feedback through an anthropomorphic avatar system," *Robotics and Autonomous Systems*, p. 104338, 2022.

[12] M. Fennel, A. Zea, and U. D. Hanebeck, "Optimization-driven design of a kinesthetic haptic interface with human-like capabilities," *IEEE Transactions on Haptics*, vol. 15, no. 1, pp. 45–50, 2021.

[13] F. Romano, Nava *et al.*, "The codyco project achievements and beyond: Towards human aware whole-body controllers for physical human robot interaction," *IEEE Robot. Automat. Lett.*, 2017.

[14] M. Alexa, "Super-fibonacci spirals: Fast, low-discrepancy sampling of so (3)," in *IEEE/CVF CVPR*, 2022, pp. 8291–8300.

[15] T. Yoshikawa, "Manipulability of robotic mechanisms," *The international journal of Robotics Research*, vol. 4, no. 2, pp. 3–9, 1985.

[16] R. Diankov, "Automated construction of robotic manipulation programs," 2010.

[17] D. Coleman *et al.*, "Reducing the barrier to entry of complex robotic software: a moveit! case study," *Journal of Software Engineering for Robotics*, vol. 5, no. 1, pp. 3–16, 2014.

[18] R. Smits. KDL: Kinematics and Dynamics Library. [Online]. Available: http://www.orocos.org/kdl

[19] Franka Emika GmbH. Robot and interface specifications. [Online]. Available: https://frankaemika.github.io/docs/control_parameters.html

[20] KUKA AG. Lbr iiwa specification. [Online]. Available: https://www.kuka.com/en-de/products/robot-systems/industrial-robots/lbr-iiwa